Superficies y Vacío **23 (2)** *6-13, junio de 2010*

©*Sociedad Mexicana de Ciencia y Tecnología de Superficies y Materiales*

Analysis of masking effect on laser light scattering from unidirectional and isotropic machined surfaces

Juan de Dios Ortiz-Alvarado, Jorge A. Huerta-Ruelas
Centro de Investigación en Ciencia Aplicada y Tecnología Avanzada Instituto Politécnico Nacional
Laboratorio de Metrología Óptica
Cerro Blanco 141 Colinas del Cimatario C.P. 76090 Querétaro, Querétaro México.

(Recibido: 19 de marzo de 2009; Aceptado: 4 de mayo de 2010)

An experimental study of masking effect on laser light scattering from machined surfaces is described. The results indicate that asperity distribution on rough surfaces is an implied factor on masking effect in addition to roughness and RMS slope. The masking effect was monitored on light scattering from isotropic and unidirectional rough surfaces. The masking effect characterized in isotropic rough surfaces agrees with the shadowing-masking function defined by B.G. Smith [IEEE Trans. Ant. and Prop. **15** 668 (1967)]. We propose a new expression defined to describe masking effect on light scattering from unidirectional machined surfaces. This function was verified by comparing with experimental data. The results and the function proposed, are useful in implementing laser light scattering instruments for on-line monitoring of surface processes which produce unidirectional surface patterns (such as turning, milling, grinding, and some cases of extrusion, lithography and thin film growth), where geometrical setup requires large incidence angle.

Keywords: Laser light scattering; Surface roughness; Shadowing effect; Masking effect; Optical roughness meter

1. Introduction

Recently, optical techniques have been introduced successfully in implementing non-destructive and non-contact systems for surface roughness inspections. There are several optical techniques applied on this task, such as laser profilometry [1, 2], which in general utilizes expensive and large equipment, and their implementation is difficult for on-line and in-situ monitoring. Laser speckle pattern analysis is another optical technique used for surface inspection [3, 4], however it requires that the test surface should be statistically isotropic. Hence speckle pattern analysis is inapplicable to rough surface measurements where specimens have preferred orientations, resulting from machining processes such as turning, milling and grinding. The Angular Distribution of Laser Light Scattering Intensity (ADLLSI) analysis overcomes these disadvantages, leading to the development of instruments for on-line monitoring of surface manufacture processes [5-8]. Laser light scattering instruments detect light intensity over a limited angular interval; therefore the set of acquired data by the instrument is named as Laser Light Scattering Pattern (LLSP). In our system the detection interval is over a limited region in the plane of incidence.

Laser light scattering instruments use two main methods for correlating LLSP with surface roughness features. The first one fits LLSP data with a physical model [9]. The most used physical model was derived by Beckmann and Spizzichino [10]. The second method is based on the assumption that LLSP has a normal distribution shape, where its variance is the correlation parameter with average roughness or RMS (root mean square) slope [11, 12]. These analyses are achieved with the assumption that LLSP is symmetric around the angular position corresponding to specular reflection. This is valid only if the angle of incidence of light beam respect to surface normal is small, then laser scattering instruments are limited due to compliance with this condition. When angle of incidence is increased, attenuation is detected on light scattered intensity at angular positions far from surface normal, and then LLSP has an asymmetric shape. This effect depends on angle of incidence, light wavelength, surface roughness and RMS slope, and is known as shadowing – masking effect.

There are surface processes with a geometric layout where a laser light scattering instrument for on-line monitoring can be installed only with a large angle of incidence (more than 45 degrees). Therefore shadowing – masking effect on LLSP analysis has to be considered within these applications.

The shadowing-masking effect is more predominant when the surface roughness value is the same order as incident light wavelength. This effect was described first by Torrance and Sparrow [17] and later by Beckmann [18] and Smith [19], who derived a function which defines the amount of attenuation detected in a specified angular position. The Smith shadowing-masking function is the most accepted and has been used in computing for generation of graphics which simulate the appearance of rough surfaces [21,22], and also in novel studies about laser light scattering from rough metallic surfaces [13]. It has been pointed out the features of LLSP from unidirectional rough surfaces [15-16], but the shadowing masking effect to explain them, has not been reported.

This paper describes a study of masking effect on LLSP from machined surfaces. The results given here indicate that Smith function is suitable in analysis of isotropic rough surface (where there is a uniform distribution of asperity over surface plane). For unidirectional rough surface which

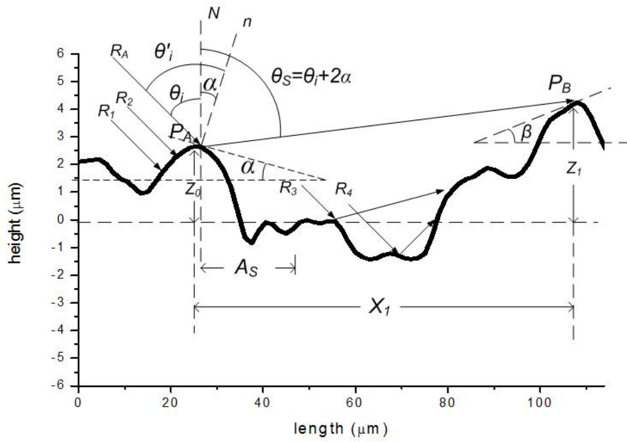

Figure 1. Geometrical description of light beams reflected by a point on a rough surface.

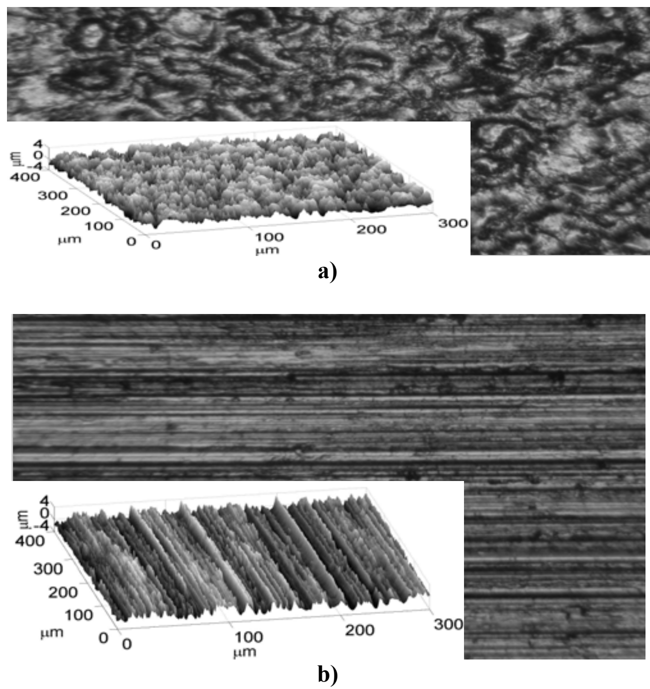

Figure 2. Photographs obtained with a metallographic microscope of: a) EMD specimen with R_a=0.813μm, and, b) Ground specimen with R_a=0.800 μm. Inset images are 3D projections from same photographs.

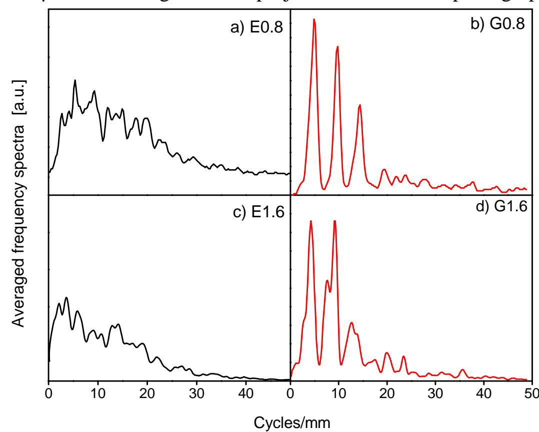

Figure 3. Averaged frequency spectra of specimens selected: a) E0.8, b) G0.8, c) E1.6 and d) G1.6.

does not fulfill assumptions considered in Smith function derivation, we propose a new function based on masking effect description on this kind of surfaces.

2. Theory

2.1. Surface roughness specifications

Mechanical profiler is the conventional instrument used to obtain surface roughness specifications. This instrument has a fine stylus which is kept in contact with surface. The stylus is displaced in a straight line trajectory parallel to surface plane. Peaks and valleys of surface topography displace the stylus in vertical direction and by means of an electromechanical system; vertical displacements are converted to an electrical signal proportional to peaks and valleys heights. The measurement obtained from profiler is known as profile, and is composed by *N* discrete data. Each z_i data corresponds to i^{th} measurement of surface height profile spaced by the sampling interval Δ_x of horizontal displacement. The equations (1) and (2) define respectively the specifications of average roughness (R_a) and RMS roughness (R_q) which are calculated from profile data.

$$R_a = \frac{1}{N}\sum_{i=1}^{N}|z_i| \quad (1)$$

$$R_q = \sqrt{\frac{1}{N}\sum_{i=1}^{N} z_i^2} \quad (2)$$

The autocorrelation function is used to describe the characteristic period of a random rough surface and it is defined as:

$$C(j) = \frac{\sum_{i=1}^{N}(z_i)(z_{i+j})}{\sum_{i=1}^{N} z_i^2} \quad (3)$$

The autocorrelation length (*T*) is calculated from (3), and is equal to value of *j* where $C(j)=e^{-1}$. An increment of one in index *j* is equal to sampling length Δ_x. The RMS slope is defined as:

$$\Delta_q = \sqrt{\frac{1}{N-1}\sum_{i=1}^{N-1}\frac{(z_{i+1}-z_i)}{\Delta_x}} \quad (4)$$

RMS slope is used as correlation parameter with LLSP [9, 11], while the model defined in [10] considers quotient R_q/T as the RMS slope. These parameters, Δ_q and R_q/T, are proportionally related as:

$$\Delta_q = \frac{\sqrt{2}R_q}{T} \quad (5)$$

points of surface topography, this is the masking effect and it produces attenuation on the light intensity detected at angular position θ_S.

Table 1. Roughness specifications of specimens obtained with a mechanical profiler.

Sample	Ra (nominal) (μm)	Ra (μm)	Δq	Rq (μm)	T (μm)
G0.1	0.1	0.0790	0.0435	0.1035	5.0
G0.2	0.2	0.1975	0.0867	0.2550	5.875
G0.4	0.4	0.3887	0.1338	0.4927	9.933
G0.8	0.8	0.7324	0.1856	0.9115	13.444
G1.6	1.6	1.4888	0.2281	1.8011	18.341
E0.4	0.4	0.3790	0.1340	0.4648	5.9437
E0.6	0.6	0.6292	0.1831	0.7701	7.1971
E0.8	0.8	0.9060	0.1734	1.1554	12.572
E1.2	1.2	1.2004	0.1800	1.5224	15.711
E1.6	1.6	1.4408	0.2019	1.7998	17.043

2.2. Light Scattering from Rough Surfaces

In general, values of R_a and R_q obtained from a standard machining process are in the order of 1μm, and if a laser light source with wavelength (λ) within visible spectrum is used for implementing scattering technique, scattering phenomenon can be described by geometrical optics with good accuracy [20]. In this model it is assumed that light flux is specularly reflected by each point of surface. Figure 1 shows a scheme for describing light scattering by geometrical optics. Incident light beam may be thought of as a collection of rays where each ray travels in a straight line in a homogenous medium. In Figure 1, ray R_A reaches the surface in P_A with an angle of incidence θ_i respect to surface normal N. The point P_A has a local normal n with an angle α respect to N. The ray is specularly reflected in P_A with an angle $\theta_S=\theta_i+2\alpha$. If statistical distribution of surface roughness is normal, local slope distribution is normal too. Therefore ADLLSI shape is approximated by a Gaussian function. The ADLLSI measured on the plane of incidence and normalized respect to intensity at angular position of specular reflection is calculated with equation (6).

$$I_N(\theta_i,\theta_S)=\frac{F(\theta_i')}{F_0}S\exp\left(-\frac{\tan^2\left(\frac{\theta_s-\theta_i}{2}\right)T^2}{2R_q^2}\right) \quad (6)$$

Where $F(\theta_i')$ is the Fresnel reflectivity at the local incidence angle θ_i'. With reference to Figure 1 $\theta_i'=\theta_i+\alpha$. F_0 is the reflectivity at θ_i of a smooth surface made of same material as analyzed rough sample. S is the shadowing-masking factor.

Rays R_1 and R_2 are obstructed to reach a region labeled as A_S. This effect is known as shadowing and is determined by θ_i and surface roughness. It is evident that by increasing θ_i this effect is increased. Rays R_3 and R_4 reach deep regions of surface and reflected rays are obstructed by higher points of surface topography, this is the masking effect and it produces attenuation on the light intensity detected at angular position θ_S.

As it was indicated, shadowing is function only of θ_i and surface roughness, therefore the attenuation on LLSP defined from comparing scattered light intensity in a defined θ_S interval with θ_i constant, is produced only by masking effect. Hence the factor S in (6) is determined only by masking if θ_i is kept constant.

The attenuation produced by shadowing and masking effect can be calculated using the function derived in [19]. This function defines a value between 0 and 1 for each angular position θ_S, it indicates the fraction of light flux which is not blocked for high points of surface topography, and is named as correspond to shadowing or masking function. The function was defined from the elementary system shown in Figure 1. The ray reflected in P_A in angular direction θ_S, is blocked by P_B if $z_1>z_0+x_1 Cot\theta_S$ and local slope ($tan\beta$) at P_B is greater than $Cot\theta_S$. Under the assumption that statistical distributions of surface roughness and local slope are normal, the masking function is determined by the evaluation of the probability that a light beam reflected in direction θ_S will not be obstructed. The masking function is defined in (7).

$$S(\theta_S)=\frac{\left(1-\frac{1}{2}erfc\left(\frac{Cot(\theta_S)T}{\sqrt{2}R_q}\right)\right)}{\left(\Lambda\left(Cot(\theta_S)+1\right)\right)} \quad (7)$$

Where:

$$\Lambda(Cot(\theta_S))=\frac{1}{2}\left(\frac{2T}{\sqrt{\pi}R_q Cot(\theta_S)}\exp\left(-0.5\left(\frac{Cot(\theta_S)T}{\sqrt{2}R_q}\right)^2\right)-erfc\left(\frac{Cot(\theta_S)T}{\sqrt{2}R_q}\right)\right) \quad (8)$$

The equation (7) defines the shadowing function by replacing θ_S by θ_i. In reference to Figure 1 and under mentioned assumptions, the probability that a light beam reflected in direction θ_S to be obstructed in an isotropic surface is less than the probability to be obstructed in a

unidirectional surface. As it can be deduced from Figure 1, in an isotropic surface points as P_B can be present or not with a probability according to a normal distribution on a line with x and z fixed. In a unidirectional surface, points like P_B are kept constant through y axis, producing a higher masking effect.

3. Materials and Methods

3.1. Specimens

Two commercial surface roughness standards sets made of nickel where used for experiments. First one is a *Flexbar 16008* (http://www.flexbar.com) which includes five unidirectional Ground specimens with R_a values from 0.1µm to 1.6µm. The other standard set is an Electrical Discharge Machined (EDM) comparator *E9* (http://www.garelectroforming.com/) which includes five electrical EDM specimens with R_a from 0.4µm to 1.6µm. EDM specimens have a homogenous distribution of roughness over surface plane, hence can be considered as isotropic surfaces, while Ground specimens have a preferred direction of roughness, therefore they are considered as unidirectional surfaces. The surface of an EDM specimen with R_a=0.813µm and Ground specimen with R_a=0.800 µm are shown in Figure 2a) and Figure 2b), respectively. Both pictures were acquired with a metallographic microscope. Inset images are 3D projections built from photographs, where ordinate scale was assigned using numerical values obtained with a mechanical profiler *SJ400™* (Mitutoyo Inc.). Specimens roughness were evaluated by analysis of profiles acquired with profiler with a stylus tip radius of 2 µm. Ten profiles with 2.4 mm length were acquired from each specimen. The scans achieved by profiler were parallel and separated by 100 µm each other. Roughness specifications calculated from profiles were averaged. In table 1 the average roughness specifications for each specimen are shown. We use prefix “*G*” to refer to Ground specimens and *“E”* for EDM specimens.

Specimens to be analyzed by laser light scattering technique were selected to form pairs composed by a Ground specimen and a EDM specimen with R_a and Δ_q similar to each other. From table 1, pairs formed by specimens G0.8 with E0.8 and G1.6 with E1.6 were selected for further analysis. The masking effect will be analyzed on LLSP, in each pair of specimens.

Before LLSP analysis, frequency spectrum analysis of the profiles shows additional differences between EDM and Ground specimens. The frequency spectrum was calculated on each of ten profiles acquired from selected specimens and were averaged to obtain a representative frequency spectrum of the specimen. Figure 3 shows averaged frequency spectrum of the pairs G0.8 (Figure 3b)) with E0.8 (Figure 3a)) and G1.6 (Figure 3d)) with E1.6 (Figure 3c)). Frequency spectrum of Ground specimens have more defined periodic components, hence a better defined characteristic periodic pattern can be identified in the profile compared with EDM specimens.

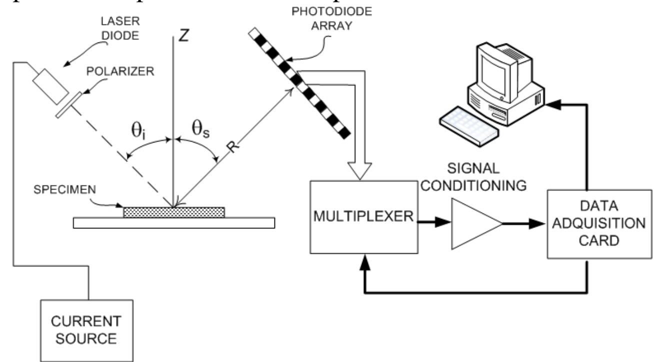

Figure 4. Scheme of laser light scattering pattern acquisition system.

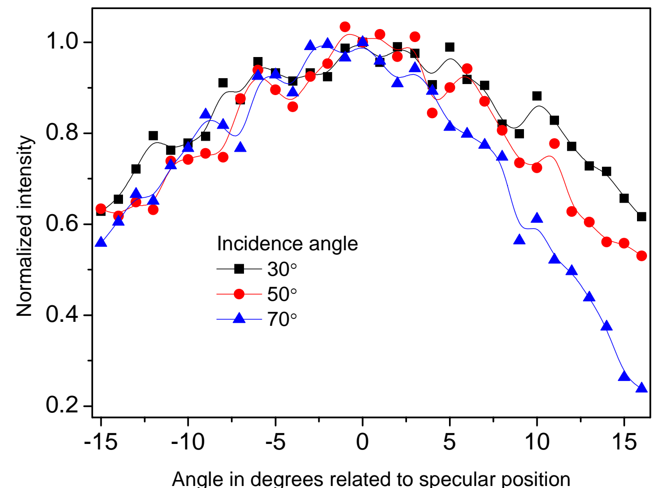

Figure 5. LLSP obtained from G0.8 specimen acquired with angle of incidence of 30º, 50º and 70º. The data are normalized respect to intensity detected in angular position of specular reflection.

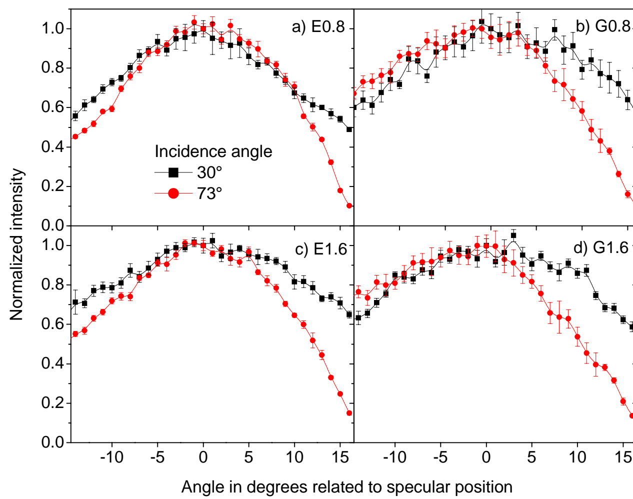

Figure 6. LLSP obtained from selected specimens with angle of incidence of 30º and 73º.

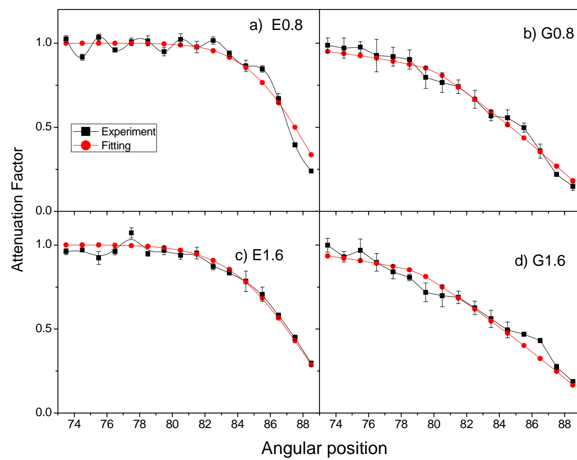

Figure 7. Fittings of EMF obtained experimentally employing the masking function of: a) and c) equation (7), and b) and d) equation (12).

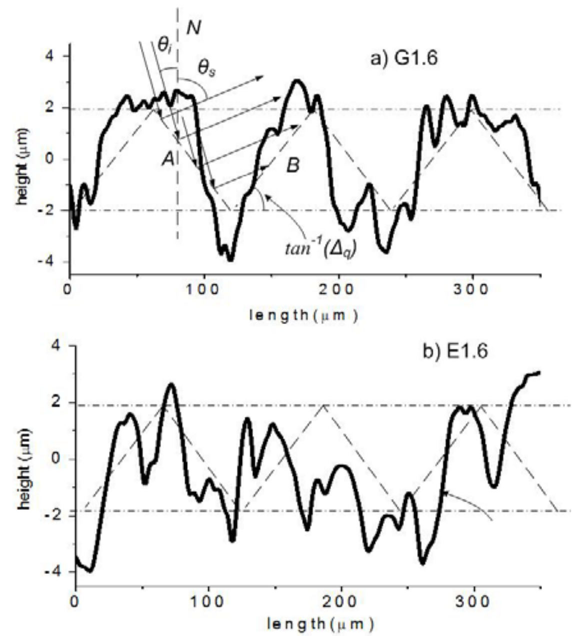

Figure 8. Approximation of the profile of rough surfaces to a triangular function with slope Δ_q, for: a) Ground specimen G1.6, b) EMD specimen E1.6.

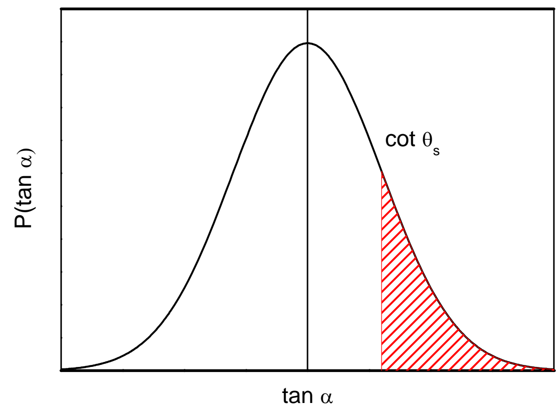

Figure 9. Relative position of complementary slope $Cot\theta_S$, within statistical distribution of local slopes in profile. The dashed area represents the probability of light beam reflected in direction θ_S to be obstructed.

3.2. LLSP Acquisition system

An instrumentation system was implemented to obtain LLSP for specimen analysis by laser light scattering technique. Experimental setup for LLSP acquisition is

shown in Figure 4. Light source is a laser diode *DL7140-201S* (Sanyo Inc.) with λ= 635 nm and 50mW power emission. Laser diode is contained in a LDM 3457 housing (Optima Precision Inc.), which includes a collimating lens for reducing light divergence. A current source LDC-202B (Thorlabs Inc.) is used as laser diode power supply. Light beam emitted by laser diode is transmitted through a polarizer to obtain an electric field oriented perpendicularly respect to incidence plane. This polarization condition minimizes reflectivity variation by θ_i changes. The LLSP is detected by a photodiode array of 32 elements built with two 16-element arrays model PDB-C216 (from *Avanced*

Photonix Inc). As can be seen in Figure 4, light scattered intensity at angular positions near specular reflection is detected by the elements of photodiode array, centered on specular reflection beam with a mechanical positioning system which allows keeping this condition even if θ_i is modified.

The electric signal generated by each photodiode of the array contains unwanted components produced by environment illumination and electric noise. In order to suppress these signals, light beam is modulated with a laser diode current source modulated in intensity at a frequency of 3 kHz. Hence signal components produced by scattered light from specimen have this frequency; therefore using a band pass filter, signal components with different frequencies can be suppressed.

A multiplexer selects sequentially the signal to be processed from photodiode array. The obtained signal proportional to light intensity is converted to a digital format and transferred to a personal computer (PC) through a high speed data acquisition card PCI6251M (*National Instruments Inc*). The PC runs software which executes the functions of additional processing, display and data storage. The software was developed in *LabView™*.

The acquired LLSP is composed by a set of 32 signal data which correspond to light intensity detected at different angular positions. Photodiode array elements are numbered as follows: First element (1st) which detects light intensity at the angular position closer to surface normal, and the 32th element farthest from the surface normal. The distance between middle element of photodiode array and surface specimen was R=91 mm. Slight attenuation on intensity detected by each element, is produced by change in orientation and distance from surface specimen due to linear shape of photodiode array, which is compensated by software of LLSP acquisition system. In this geometry each element of photodiode array detects light intensity within interval close to a 1.0º range. The incidence angle θ_i=73º is the maximum value in which all elements of the photodiode array detect scattered light, this is equivalent to an angular interval from θ_S=57º (detected by 1st element) to θ_S= 89º (detected by 32th element). We calculate, an Estimated Masking Function (EMF) obtained from LLSP by dividing one by one the intensity detected by the 16 elements in angular positions $\theta_S>\theta_{i,}$ by the intensity detected from symmetric opposite elements at angular positions $\theta_S<\theta_{i.}$

There is an additional variation in intensity on LLSP by Fresnel reflectivity angular dependence. Considering that geometric optics light flux reflected in angle θ_S is related to local incidence angle θ_i', the EMF is calculated with (9), where I_i is the intensity detected by the ith photodiode, and F_i is the Fresnel reflectivity corresponding to angle θ_i' defined by angular position θ_S of ith photodiode:

$$S_i = \left(\frac{I_{i+16}}{I_{17-i}}\right)\left(\frac{F_{17-}}{F_{i+1(}}\right) \qquad (9)$$

The described system acquires LLSP in a linear angular interval from incidence plane, and can be applied to analyze isotropic and unidirectional surfaces. The data set to be processed is minimum compared with data provided by a CCD sensor, and can be processed in a shorter time. This feature makes suitable the system application in on line monitoring where is required to process data at high speed and to suppress disturbances by environment illumination and electromagnetic induction present in most industry environments.

4. Results

The LLSP from G0.8 specimen acquired at angle of incidence of 30º, 50º and 70º is shown at Figure 5. It can be seen that attenuation effects on angular position far from specular reflection is increased as θ_i is increased. LLSP are normalized respect to the intensity detected at specular reflection position to compare their shape. The LLSP acquired with θ_i=30º has a symmetric shape around the angular position of specular reflection. It can be seen in LLSP acquired with θ_i=50º and θ_i=70º, that the attenuation produced by masking effect intensify as the incidence angle increases.

A set of LLSP was acquired from selected specimens with θ_i=30º and θ_i=73º in ten points over their surface and averaged. Averaged LLSP from specimens are shown in Figure 6. LLSP were normalized respect to intensity detected in angular position of specular reflection. LLSP acquired with θ_i=30º show a more symmetric shape, in contrast with LLSP obtained with θ_i=73º which show a less symmetric shape produced by a masking effect. Difference in intensity between LLSP for θ_i=30º and θ_i=73º angles, begin to change at angles closer to specular position for ground specimens (Figure 6b) and Figure 6d)) compared with EMD specimens (Figure 6a) and Figure 6c)). Additionally, a smoother behavior is found in Ground specimens compared with EMD specimens, and could be related to a more feasible averaged diffraction phenomena related to a higher degree of surface order in one direction (grating like behavior) [14].

The validity of equation (7) for describing masking effect from Ground and EMD surfaces was tested. This was achieved by fitting to equation (7) the EMF obtained from LLSP with θ_i=73º. Least squares algorithm was applied for fitting. From this operation we obtained Δ_q=0.151 for specimen E0.8, and Δ_q=0.176 for specimen E1.6, these values are close to Δ_q values obtained by mechanical profiler indicated in table 1. In Figures 7a) and 7c) fittings of EMF to equation (7) from EMD specimens are shown. Fitting EMF with equation (7) from Ground specimens (not shown in Figure 7), gives Δ_q=0.447 for specimen G0.8, and Δ_q=0.486 for specimen G1.6, which have a considerable error respect to Δ_q indicated in table 1. Therefore we propose in this paper, a new function to describe attenuation on LLSP from unidirectional rough surfaces. Derivation of masking function is achieved considering the probability of a ray reflected in scattering angle θ_s will not

be obstructed. This is the same assumption considered in Smith function derivation. We assume that probability of occurrence of two independent events determine masking effect.

First one is produced by periodic shape of surface profile. The periodicity can be represented by a periodic triangular function with slope equal to Δ_q, considering that this can be a correlation parameter. In Figure 8a) the periodic shape of a segment of the profile from specimen G1.6 is plotted, we can see a more defined periodicity compared to a segment of the profile from specimen E1.6 shown in Figure 8b). Light reflection in this representation is described similarly by a facet model proposed by Torrance and Sparrow [17]. As shown in Figure 8a), incident light flux is reflected by facet labeled *"A"* and is partially obstructed by adjacent facet labeled *"B"*. The fraction of light flux reflected in angular direction θ_S which is not obstructed (equivalent to probability not to be obstructed), is calculated as equation (10). This function was derived from a facets model in ref [17].

$$S_P(\theta_S) = \min\left\{1, \frac{2Cos\left(\tan^{-1}(\Delta_q)\right)Cos(\theta_S)}{Cos\left(\theta_S - \tan^{-1}(\Delta_q)\right)}\right\} \quad (10)$$

Second event that produces masking effect is determined by the probability that a reflected ray be obstructed by profile regions which their local slope is greater than complementary slope $Cot\theta_S$. In Figure 9 is shown the position of $Cot\theta_S$ respect to a statistical distribution of local slopes from profile points. The probability that a light beam reflected in angular direction θ_S for not to be obstructed, is equivalent to 1-0.5**erfc*($Cot\theta_S/(\Delta_q 2^{1/2})$). The term 0.5**erfc*($Cot\theta_S/(\Delta_q 2^{1/2})$) is equivalent to the integral in the interval $Cot\theta_S > tan\alpha < \infty$ represented by dashed area in the normal distribution shown in Figure 9. The equation (11) defines the probability of a reflected ray will not be obstructed by profile with local slope greater than $Cot\theta_S$.

$$S_D(\theta_S) = \left(1 - 0.5 * erfc\left(\frac{Cot\theta_S}{\sqrt{2}\Delta_q}\right)\right) \quad (11)$$

The joint probability of a reflected ray will not be obstructed by simultaneous occurrence of two described events is equivalent to the amount of reflected light flux which is not obstructed, and is obtained by the product of probability functions defined with equations (10) and (11). Masking function for unidirectional rough surfaces is defined in (12).

$$S(\theta_S) = S_P(\theta_S)\left(1 - 0.5 * erfc\left(\frac{Cot\theta_S}{\sqrt{2}\Delta_q}\right)\right) \quad (12)$$

Figure 7b) and 7d) show a comparison between EMF from Ground specimens fitted with equation (12). The value Δ_q obtained by fitting with equation (12) the EMF obtained from Ground specimens are Δ_q= 0.188 for specimen G0.8, and Δ_q=0.206 for specimen G1.6, these values are close to Δ_q values indicated in table 1. These results show good correlation between the proposed function and experimental data from Ground specimens. Comparing traditional masking function of EMD specimens with new masking function of Ground specimens, a clear difference in behavior can be observed, thus justifying the new expression proposed to describe unidirectional roughness patterns which exhibit higher attenuation.

Validity of model is restricted to surfaces with statistical distribution of roughness approximately normal, and a profile with a characteristic periodicity. These conditions are fulfilled by most surfaces obtained from machining processes based on chip removal by cutting tool. Some examples of high industrial importance is turning and milling processes.

5. Conclusion

An experimental study of masking effect on laser light scattering from machined surfaces was described. The obtained results indicate that this effect is dependent on the fashion that asperity on surface is distributed besides roughness and RMS slope, main variables taken into account in available models. Isotropic and unidirectional surfaces were studied. It was tested that for isotropic surfaces Smith function is suitable to predict light intensity attenuation by masking effect on large scattering angles. In unidirectional surfaces attenuation rate by masking is greater and the function defined in this work describes phenomena with better approximation. Methodology developed can be applied to different roughness ranges and pattern surface shapes. Function to compensate masking effect can change but procedure had already defined in this work.

Finally, these results are important considerations for laser light scattering instrument design to be applied at large incidence angles. Different functions could be programmed if instrument is designed to be applied in several processes. In particular, the system built for this study, can be used with a few changes to characterize additional phenomena present for others surface morphologies obtained in custom machine shop, but also can be applied to processes like extrusion or anisotropic thin films growth techniques like sputtering, MOCVD or MBE, with adaptations, according to their surface roughness range. It is remarkable from this system, its high speed, non invasive and immune to noise sources, making suitable to operate in harsh environments like those found in industry and mechanical shops for quality control.

Acknowledgements

This work was supported by CONACYT under project SEP-2004-C01-47938. Authors acknowledge to Arturo

Moreno Baez with his help to implement mechanical positioning system. Also, it is recognized a fruitful discussions with Ph.D. Gerardo Miramontes de León and Ph.D. Ivan Dominguez López.

References

[1]. R. Shinozaki, O. Sasaki and T. Suzuki. Advanced Materials and Devices for Sensing and Imaging. Proceedings of SPIE **5633**, 31 (2005).

[2]. P. Tomassini, L. Rovatti, G. Sansoni, and F. Docchio, Review of Scientific Instruments **72**, 2207 (2001).

[3]. M.A. Seif and M. Rawwash, Journal of Testing and Evaluation **34,** 1 (2006).

[4]. I. Yamaguchi, K. Kobayashi and L. Yaroslavsky, Optical Engineering **43,** 2753 (2004).

[5]. J. G. Valliant, M. P. Folley and J. M. Bennett, Optical Engineering **39**, 3247 (2000).

[6]. D. Fontani, F. Francini, G. Longobardi and P. Sansoni, Optics and Lasers in Engineering **35**, 387 (2001).

[7]. C.J. Tay, S.H. Wang, C. Quan and H. M. Shang, Optics Comunications **218,** 1 (2003).

[8]. M. Lequime, M. Zerrad, C. Dummié and C. Amra, Optics Communications **282**, 1265 (2009).

[9]. E. Marx and T. V. Vorburger, Applied Optics **29,** 3613 (1990).

[10]. P. Beckmann, A. Spizzichino, The Scattering of Electromagnetics Waves from Rough surfaces, (Pergamon Press. London 1963).

[11]. L. Cao, T.V. Vorburger, A.G. Lieberman and T.R. Lettieri, Applied Optics **30**, 3221 (1991).

[12]. S.H. Wang, C. Quan, C. J. Tay and H. M. Shang, Optical Engineering **39**, 1597 (2000).

[13]. H. Li and K.E. Torrance, Advanced Characterization Techniques for Optics, Semiconductors, and Nanotechnologies II, Proceedings of SPIE **5878**, 58780V (2005).

[14]. C. Babu Rao and A.V. Ananta Lakshmi, Applied Optics **37**, 7305 (1998).

[15]. V.Y. Mendeleyev, Optics Communications **268**, 7 (2006).

[16]. J. D. Ortiz-Alvarado, J. A. Rodríguez-Tirado, J.A. Huerta-Ruelas, Determinación de acabado superficial mediante patrón asimétrico de luz láser esparcida en superficies maquinadas, 28th International Conference on Materials Surfaces and Vacuum, (2008).

[17]. K. Torrance and E. Sparrow, Journal of the Optical Society of America **57**, 1105 (1967).

[18]. P. Beckmann, IEEE Transactions on Antennas and Propagation **AP-13**, 384 (1965).

[19]. B.G. Smith, IEEE Transactions on Antennas and Propagation **AP-15**, 668 (1967).

[20]. K. Tang, R. A. Dimenna and R.A. Buckius, International Journal of Heat and Mass Transfer **40**, 49 (1997).

[21]. X.D. He, K. Torrance, F. X. Sillion, and D.P. Greenberg, Computers Graphics **25**, 175 (1991).

[22]. B Walter, S.R. Marschner, H. Li, K. E. Torrance, "Microfacet Models for Refraction through Rough Surfaces", Eurographics Symposium on Rendering 195 (2007).